crystals

MDPI

Article

Comparative ^{2}H NMR and X-Ray Diffraction Investigation of a Bent-Core Liquid Crystal Showing a Nematic Phase

Maria Ghilardi [1], Fabrizio C. Adamo [2], Francesco Vita [2,*], Oriano Francescangeli [2] and Valentina Domenici [3,*]

1 Dipartimento di Chimica e Tecnologie Farmaceutiche, Università di Pisa, 56124 Pisa, Italy
2 Dipartimento di Scienze e Ingegneria della Materia, dell'Ambiente ed Urbanistica, Università Politecnica delle Marche, 60131 Ancona, Italy
3 Dipartimento di Chimica e Chimica Industriale, Università di Pisa, 56124 Pisa, Italy
* Correspondence: f.vita@univpm.it (F.V.); valentina.domenici@unipi.it (V.D.); Tel.: +39-071-2204223 (F.V.); +39-050-2219-215 or +39-050-2219-267 (V.D.)

Received: 14 March 2020; Accepted: 7 April 2020; Published: 9 April 2020

Abstract: Bent-core liquid crystals showing a nematic phase stable at low temperatures are very attractive for applicative purposes in view of the inherent biaxial nature of the nematic phase. In this work, a typical five-ring bent-core mesogen was investigated by means of ^{2}H NMR spectroscopy and X-ray diffraction (XRD) methods. These techniques provide complementary information on the structural properties of the nematic phase and the average mesogen conformation: small-angle XRD reveals the presence of short-range positional order in the form of skewed cybotaxis, while a comparison of the orientational order parameters measured by wide-angle XRD and NMR provides an estimate of the molecule bend angle. In addition, ^{2}H NMR puts in evidence the occurrence of an unexpected transition to a low-temperature tilted phase, having a crystalline or smectic-like character. The results were compared with those of previous ^{13}C NMR investigations.

Keywords: bent-core liquid crystal; nematic phase; cybotaxis; ^{2}H NMR; X-ray diffraction

1. Introduction

Bent-core liquid crystals (BLCs) were first discovered in 1996 [1], and they are still very attractive for fundamental scientific reasons and for their potential applications, as demonstrated by very recent works [2–4]. Several reviews have been published describing the peculiar smectic phases formed by BLCs, such as the typical *B2* phase, characterized by ferro- and anti-ferroelectric, synclinic and anticlinic behaviours, or the *B7* phase, showing a helical supramolecular structure [5–7]. However, in the last twenty years, BLCs have attracted increasing attention also in view of the unusual properties of their nematic phase [8]. For instance, since 2004, several groups tried to demonstrate the inherent mesophase biaxiality of nematic phases formed by bent-core mesogens [9–11]. To this purpose, several experimental methods have been used, including polarizing optical microscopy and conoscopy, Deuterium Nuclear Magnetic Resonance (^{2}H NMR) spectroscopy and X-ray diffraction (XRD). In some cases, the biaxial symmetry of the molecular arrangement of nematic phases formed by BLCs was induced by the presence of electric fields; in others, an extraordinary phase sensitivity to magnetic fields was observed [12–14]. In any case, there is a lot of evidence that the unconventional properties of BLCs' nematic phase are related to the short-range organization of bent molecules and to the presence of smectic-like nanodomains [15–18]. This behaviour has been associated to the '*cybotactic*' feature of the nematic phases formed by bent-core liquid crystals. The term '*cybotactic nematic*', introduced for the first time in 1970 by Adrian de Vries [19], indicates the occurrence of a a stratified supramolecular

structure in nematic domains, which, in BLCs, is not due to pre-transitional local fluctuations in the vicinity of a nematic-smectic phase transitions. Indeed, the accepted model of the biaxial '*cybotactic nematic*' phase assumes the existence of a peculiar short-range ordering in the form of nanometer-sized clusters having a layered supramolecular structure (usually tilted, i.e., smectic C-like) with intrinsic biaxial orientational order [15]. The main evidence of this '*cybotactic*' local arrangement is given by the characteristic four-spot small-angle (SA) X-ray XRD feature [15–18], which is sensibly different from the two-spot pattern exhibited by conventional calamitic nematics.

The occurrence of nano-sized aligned domains or local clusters in the nematic phase of bent-core LCs was also supported by independent studies based on Dynamic Light Scattering (DLS) [20] and on a combination of NMR experiments performed on similar five-rings banana-shaped molecules [21–23]. In particular, ^{2}H NMR static spectra recorded in the isotropic and in the nematic phase of these BLC nematogens were characterized by an unusual line-broadening [24], related to both dynamic and static reasons, which were further investigated by means of ^{2}H NMR relaxation times [25], ^{1}H NMR relaxometry [26] and ^{1}H NMR diffusometry [27]. All these studies supported the occurrence of local nanosized ordered domains, or clusters, in the isotropic and in the nematic phase formed by this type of BLC nematogens [24]. Additional ^{2}H NMR studies on molecular probes having a similar structure than the BLC aromatic core (five- or three-rings moieties), dissolved in different nematic phases, confirmed the peculiar ordering properties of BLCs [28,29]. Recent reviews have been published where the main orientational and dynamic properties of nematic phases of typical calamitic LCs and five-rings bent-core liquid crystals were compared [30,31]. Moreover, NMR spectroscopy has been used to investigate the mesophase biaxiality in several types of LC systems [32–34], such as organosiloxane tetrapodes and dendrimers [35].

In this work, a bent-core liquid crystal having a five-ring core [36] with a nematic phase stable at relatively low temperatures was investigated by means of ^{2}H NMR and XRD methods. BLCs of the same series [36] have been already studied by means of ^{13}C NMR spectroscopy [37–39] in order to get insight into both orientational and conformational properties. Here, the complementary information provided by ^{2}H NMR and XRD is used to evaluate the nematic phase orientational order parameter as well as to evidence the presence of a short-range positional order (skewed cybotaxis). A comparison of ^{2}H NMR and XRD data provides an estimate of the molecular bend angle while ^{2}H NMR data reveal an unexpected transition to a low temperature tilted phase, probably crystalline or smectic-like.

2. Materials and Methods

2.1. Liquid Crystalline Sample and Mesomorphic Characterization

The molecular structure of the deuterated bent-core liquid crystal 4,6-dichloro-1,3-phenylenebis-[4'-(9-decenyloxy)-1,1'-biphenyl] carboxylate, labelled **10DClPBBC-d$_4$**, is reported in Scheme 1.

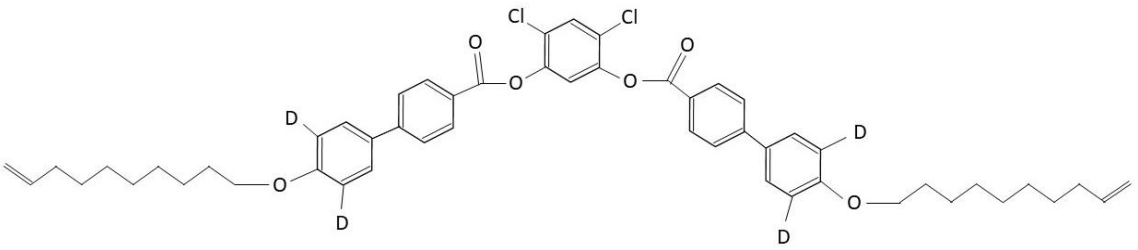

Scheme 1. Molecular structure of the bent-core mesogen labelled **10DClPBBC-d$_4$**.

This compound was synthesized according to the procedure reported in [36] and its mesomorphic behaviour was investigated by means of polarized optical microscopy (POM) and differential scanning

calorimetry (DSC), giving rise to the following mesophases' sequence (from DSC, obtained by cooling the sample at 10 °C/min rate):

Isotropic—104 °C—*Nematic*—62 °C—*Crystal*

A slightly different mesomorphic behavior, including transitions between different crystalline phases (isotropic—98.8 °C—nematic—87.6 °C—crystal$_1$—72.2 °C—crystal$_2$—51.9 °C—crystal$_3$), has been reported in the literature for the not-deuterated mesogen [36–38]. This difference may be due to the selective deuteration on the two biphenyl moieties in our compound (see Scheme 1). However, we also notice that ^{13}C NMR data in [37,38] are actually in contrast with the last-mentioned phase sequence, indicating a nematic range which essentially matches the one provided by DSC for our deuterated compound. This uncertainty of the phase diagram suggests a mesomorphic behaviour which is very sensitive to external factors, such as heating/cooling conditions, thermal history, impurities, etc. The bent-core mesogen **10DClPBBC** was previously investigated by means of ^{13}C NMR spectroscopy [37–39] and preliminary DFT calculations [40], thus indicating that the most probable conformer in the liquid crystalline phase is not planar, but it is characterized by a propeller-like structure.

2.2. H NMR Measurements

^{2}H NMR static experiments on the **10DClPBBC-d$_4$** sample were first carried out on the Infinity Plus 400 Varian, working at a ^{2}H Larmor frequency of 61.39 MHz [41]. The spectra presented in this paper were acquired with a quadrupolar echo pulse sequence, with a 90° pulse of 4.60 μs, a relaxation delay of 1 s and a quadrupolar echo delay of 20 μs. The number of scan ranged from 7000 to 50,000, depending on the type of measurements. Spectra were acquired either with or without proton decoupling. These measurements were also repeated by using the Bruker Avance II spectrometer with ^{2}H Larmor frequency of 61.40 MHz. In all cases, the bent-core LC sample was microscopically aligned within the magnet by slow cooling from the isotropic phase and the spectra were recorded either by cooling or heating the sample, with different heating and cooling rates. A simple sketch of the NMR set up is shown in Figure 1. The temperature was stable within 0.1 °C. Spectral parameters were analyzed by using the Mathematica 5.2 (Copyright 1988–2003, Wolfram Research, Inc., Oxfordshire, United Kingdom) software for PC, Kaleidagraph 3.5 (Synergy Software, Reading, PA, USA) and Excel software (Microsoft Office 10, USA) for PC.

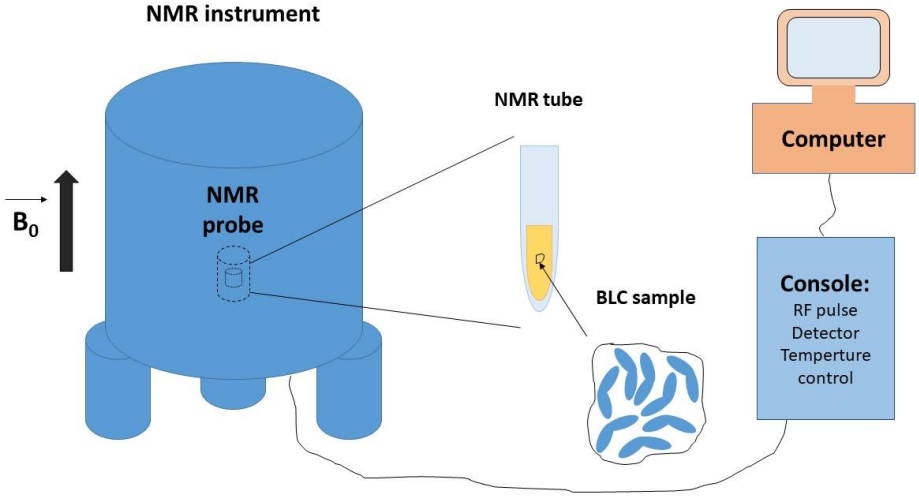

Figure 1. Experimental set-up for NMR measurements. The sample is introduced in a NMR tube, inside the NMR probe and aligned by the vertical magnetic field $\mathbf{B_0}$.

2.3. XRD Measurements

XRD measurements were carried out at the BM26B DUBBLE beamline of the ESRF using a beam energy of 12 keV (corresponding to a wavelength λ = 1.03 Å). The sample was placed in a glass capillary (1 mm diameter) and mounted in a hot stage featuring a thermal stability of ±0.1 °C. A magnetic field B = 2 T (measured in air), generated by a nitrogen-cooled superconducting magnet [42], was applied to the sample to align the molecular director **n** orthogonally to the X-ray beam. Two different set-up configurations were used for wide-angle (WA) and SA measurements: the former featured a FReLoN CCD camera placed at d = 208 mm from the sample; the latter, a Pilatus 1M photon-counting detector placed at d = 1450 mm from the sample with a vacuum tube placed in between to reduce air scattering. Measurements were carried out at discrete temperatures on cooling from the isotropic melt in steps of 5 °C and allowing the sample to equilibrate at each set point. A sketch of the experimental set-up is shown in Figure 2.

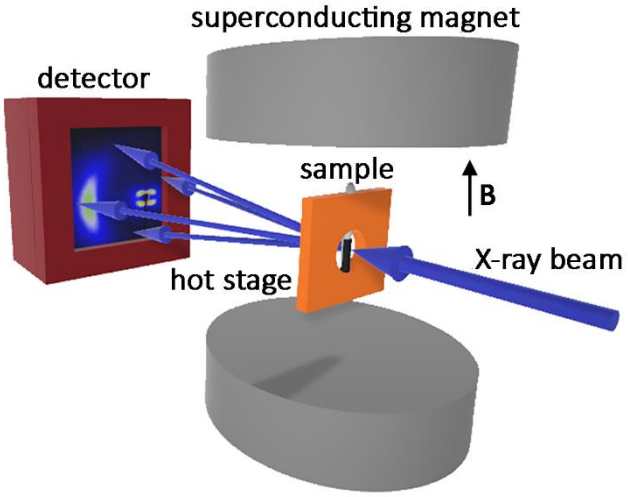

Figure 2. Experimental set-up for XRD measurements. The samples, placed in capillaries and mounted in the hot-stage, are aligned by a vertical magnetic field **B**. For small-angle measurements, characterized by a larger sample-to-detector distance, a vacuum chamber was placed between the sample and the detector to get rid of air scattering.

3. Results and Discussion

3.1. ^2H NMR Results

A selection of ^{2}H NMR static spectra of the **10DClPBBC-d$_4$** sample, obtained by applying a ^{1}H-decoupling, is reported in Figure 3. In particular, a stackplot of ^{1}H-decoupled ^{2}H NMR static spectra of the **10DClPBBC-d$_4$** sample, recorded by cooling the sample from the isotropic phase is reported in Figure 3A from T = 107 °C to 98 °C (every 1 °C) and in Figure 3B from T = 98 °C to 71 °C (every 3 °C). The ^{2}H NMR spectra in the nematic phase are characterized by a relatively sharp and intense doublet in the central region of the spectrum and a doublet with very low intensity with a larger quadrupolar splitting. These small signals are probably due to some impurities, ascribable to the same molecule with deuterons on different sites with respect to the **10DClPBBC-d$_4$** compound.

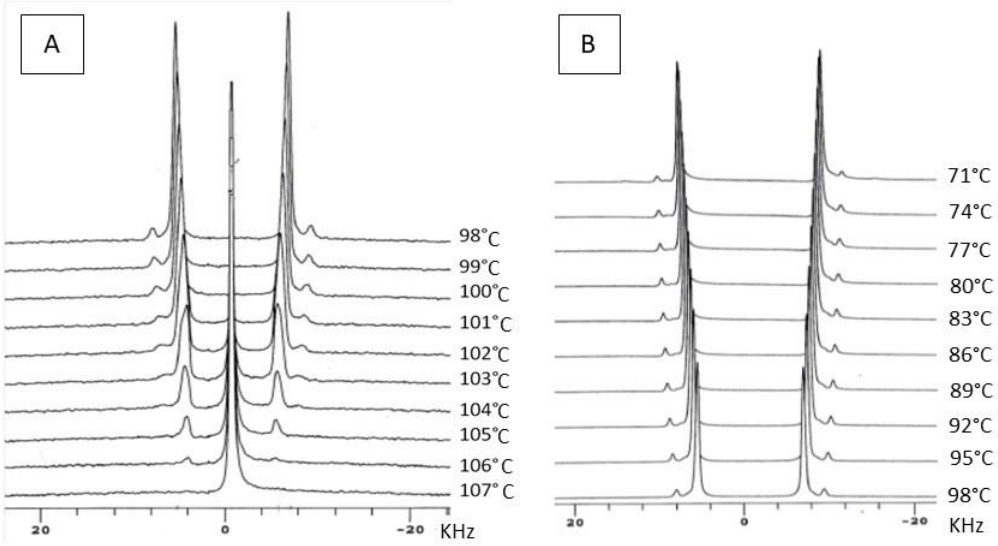

Figure 3. Stackplot of ^{1}H-decoupled ^{2}H NMR static spectra of the **10DClPBBC-d$_4$** sample, recorded by cooling the sample from the isotropic phase: (**A**) from T = 107 °C to 98 °C (every 1 °C) and (**B**) from T = 98 °C to 71 °C (every 3 °C).

As noted in Figure 3A, there is a relatively large temperature interval of the biphasic region, where both the isotropic peak and quadrupolar doublets coexist. Focusing on the more intense signals, at T < 101 °C, both the ^{2}H NMR spectral shape and line width indicate that the nematic phase is well aligned in the magnetic field, with a conventional alignment [43,44]. Moreover, in the range between 101 °C and 71 °C, the quadrupolar splitting increases by decreasing the temperature, thus indicating a progressive increase of the orientational order parameter referred to the deuterated moieties. At T < 70 °C, the ^{2}H NMR spectra are characterized by broader signals and the quadrupolar splitting starts decreasing by decreasing the temperature, thus indicating an apparent decrease of the orientational order, typical of tilted phases. A further transition, ascribable to the occurrence of a crystalline phase, appears at about 62–60 °C. Analogous measurements were acquired without ^{1}H decoupling. In this case, the spectra are much broader due to the ^{1}H-^{2}H dipolar coupling; however, the amount of dipolar splitting is detected to be quite small in the whole mesophasic range. This can be seen, for instance, in Figure 4A, where ^{2}H NMR spectra of the **10DClPBBC-d$_4$** acquired without ^{1}H decoupling, by heating the sample from the crystal phase (in the Figure, from T = 60 °C to T = 99 °C), are reported.

It should be noted that the phase transition temperatures observed by heating the sample from the crystalline phase are different from those obtained by cooling the sample. This is due to the intrinsic metastability of the mesophases and to the phenomenon of super-cooling. Focusing on the ^{2}H NMR spectra reported in Figure 4A, it is interesting to observe the significant change of the spectral features between T = 75 °C and T = 78 °C. At lower temperatures, the ^{2}H NMR spectra are very broad (line-width at half-height > 3000 Hz) and the splitting decreases by decreasing the temperatures, while at higher temperatures, the signals are much sharper (line-width at half-height < 1000 Hz) and more intense, with an opposite trend of the quadrupolar splitting versus temperature. As reported in Figure 4B, deuterons directly probe the average orientation of the two lateral wings (in particular, the two biphenyl para axes, z_{b1} and z_{b2}). The fact that a sole quadrupolar splitting is observed means that the orientation of the two lateral wings is averaged out due to fast motions (at least in the higher temperature interval). This is in agreement with previous ^{13}C NMR investigations, where single relatively sharp signals were observed for different ^{13}C sites of the BLC molecule [37–39]. As will be discussed in the last section, ^{2}H NMR actually provides information about the overall averaged

orientation of these two wings with respect to the external laboratory frame (aligned with the magnetic field) as a function of temperature.

The evidence of a tilted average orientation of the deuterated lateral wings at lower temperatures (T < 75 °C) could be associated to the occurrence of a more rigid phase, with local micro-domains having a crystalline or smectic-like character, as sketched in Figure 4B. The abrupt increase of the spectral line-broadening suggests that this phase could correspond to a crystalline phase, as noted from previous ^{13}C NMR studies [37–39]. From the ^{2}H NMR point of view, the observed spectral features can be indeed interpreted in terms of an additional phase transition between a non-tilted nematic phase (at higher temperatures) and a tilted smectic-like phase or crystalline phase (at lower temperatures).

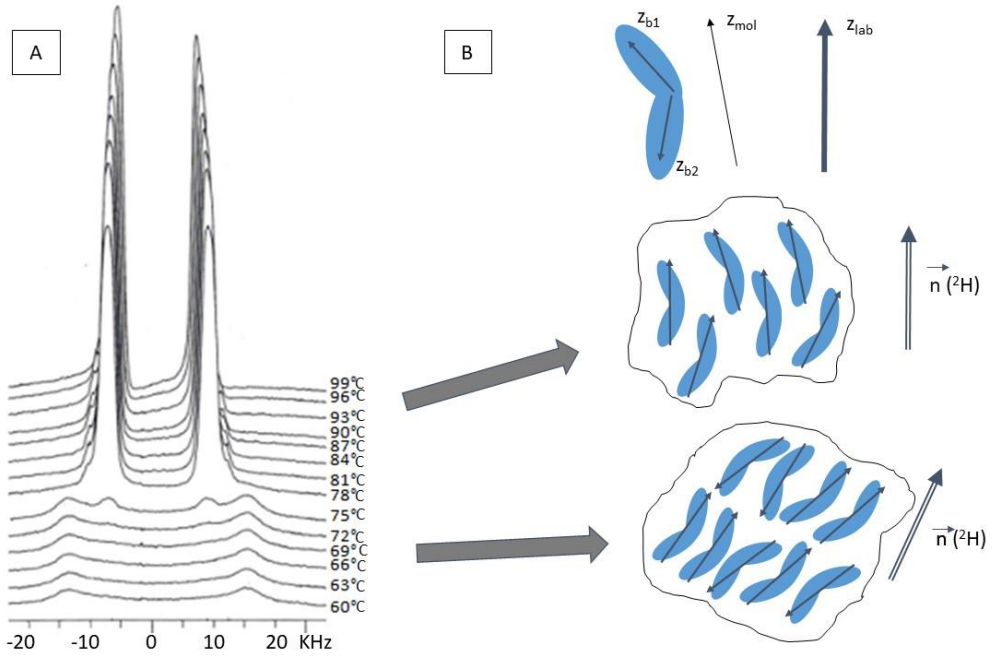

Figure 4. (**A**) Stackplot of ^{2}H NMR static spectra of the **10DClPBBC-d$_4$** sample, recorded by heating the sample from the crystal phase, without ^{1}H decoupling. Measurements were performed from 60 °C to 99 °C every 3 °C. Note the biphasic spectrum at T = 75 °C. (**B**) Sketch of a local micro-domain of bent molecules and the relative average orientation of their molecular axis according to ^{2}H NMR results, in the nematic phase, at high temperatures, and in a smectic-like or crystalline-like phase, at low temperature, as discussed in the text. The orientation of relevant axes is indicated by black arrows, as described in the text.

The quantitative analysis of the temperature-dependence of ^{2}H NMR quadrupolar splitting ($\Delta\nu_q$) can be done by using Equation (1) [30,31], which expresses the relationship between the measured quadrupolar splitting of deuterons on the aromatic fragment and the fragment orientational order parameters, S_{zz} and Δ_{biax} (= $S_{xx} - S_{yy}$), in the biphenyl axes frame (with z parallel to the para axis):

$$\Delta\nu_q = \frac{3}{2}q_{aa}\left\{S_{zz}\left(cos^2\phi - \frac{1}{2}sin^2\phi - \frac{\eta}{6}cos^2\phi + \frac{\eta}{6} + \frac{\eta}{3}sin^2\phi\right) + \Delta_{biax}\left(\frac{1}{2}sin^2\phi + \frac{\eta}{6}cos^2\phi + \frac{\eta}{6}\right)\right\} \quad (1)$$

where η is 0.04 and q_{aa} is 185 kHz, according to the literature for aromatic deuterons [30]. The angle ϕ between the C–D bond and the *para* axis of the biphenyl fragment is fixed to 60°. In the present case, we assumed the biphenyl biaxiality parameters, Δ_{biax}, to be a constant within the temperature range of stability of the mesophases. The average value of 0.037 was estimated by considering both the ^{2}H quadrupolar splitting and the ^{1}H-^{2}H dipolar splitting at few temperatures in the non-tilted phase, where it was possible to measure both quantities from the ^{2}H NMR spectrum. On the other hand, this value is in agreement with that obtained in other LC systems with deuterons on the biphenyl

moiety [30,31,43–46]. The trend of S_{zz} as a function of temperature (referred to the average local biphenyl axes of the two deuterated lateral wings) obtained by using Equation (1), is reported in Figure 5a.

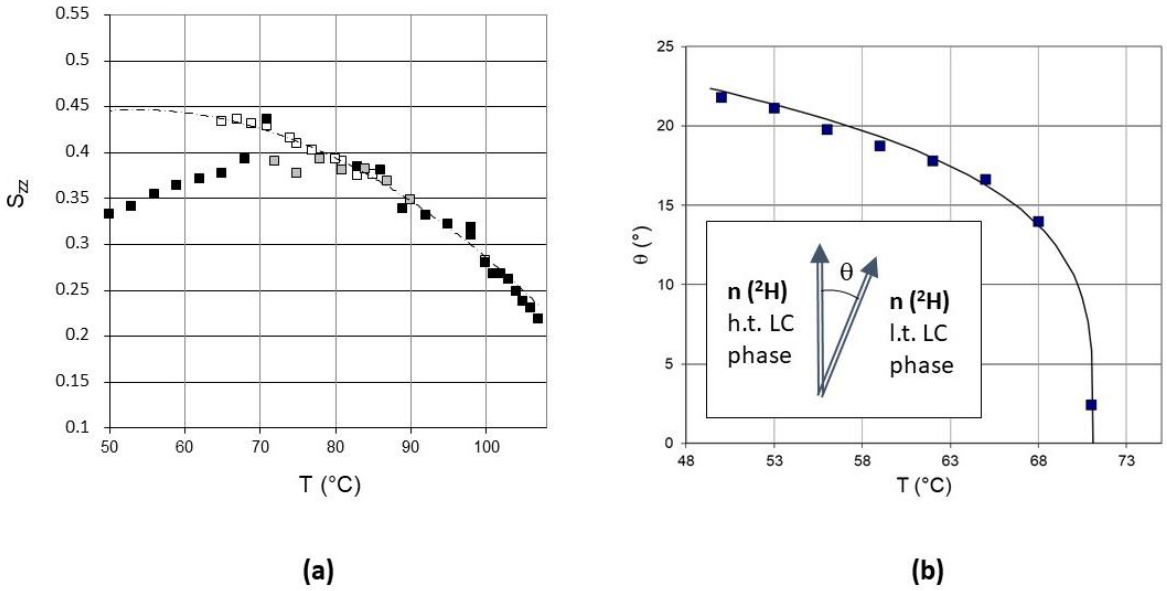

Figure 5. (**a**) Trend of the orientational order parameter S_{zz}, referring to the biphenyl para axes, as a function of temperature (T/°C), determined by analyzing the ^{2}H NMR spectra. The empty squares refer to data obtained from ^{1}H-decoupled ^{2}H NMR spectra, black full squares and grey full squares to data obtained from ^{2}H NMR spectra acquired without ^{1}H decoupling, on cooling and on heating the sample, respectively. The dashed curve corresponds to the extrapolation from the high temperature aligned phase to low temperature tilted phase. (**b**) Trend of the average tilt angle, θ, in the low temperature titled phase. The black curve corresponds to the best fitting curve by using Equation (3), as described in the text. In the inset, the angle θ is defined showing the relative orientation of the average director, as detected by ^{2}H NMR in the low temperature (l.t.) and high temperature (h.t.) LC phases.

Above 70 °C, the relatively small values of S_{zz} (<0.5) are consistent with the orientational order typical of an aligned nematic phase, once the bent geometry of the molecule is taken into account (see final discussion). The values of S_{zz} obtained in the nematic (not-tilted) phase from the ^{2}H NMR analysis are quite in agreement with those obtained for the biphenyl fragments from ^{13}C NMR studies [37–39]. The orientational order of the lateral wings of the same BLC molecule, calculated from the temperature trend of the chemical shift anisotropy of different carbon sites in combination with DTF investigations [38], was found to be smaller than that of the central ring and to reach a value $\lesssim$ 0.50 at T ~ 60 °C.

At temperatures lower than 70 °C, the decrease of S_{zz} suggests the occurrence of a tilted phase, with the magnetic field forming an angle θ with the average orientation of the lateral wings and hence, with the molecular director **n**. The temperature-dependence of S_{zz} shown in Figure 5a was analyzed in order to calculate the tilt angle, θ, between the high temperature (aligned) phase and the low temperature (tilted) phase. In particular, the comparison between the experimental values of the order parameters obtained at lower temperatures (S_{zz}^{exp}) and those extrapolated from the values obtained at higher temperatures (S_{ZZ}^{calc}) (see also the dashed curve in Figure 5a), allowed us to obtain the tilt angle, according to the following equation [43,44]:

$$S_{zz}^{exp} = S_{ZZ}^{calc}\left(\frac{3cos^2\theta - 1}{2}\right) \quad (2)$$

Moreover, the values of the tilt angle can be modelled according with the generalized Landau-de Gennes relationship [30,31]:

$$\theta = \theta_0 \left[\frac{T_0 - T}{T_0} \right]^{\gamma} \quad (3)$$

where T_0 is the temperature at which a drastic change in the spectral features is observed (T = 71.1 °C), and the parameters γ and θ_0 are best fitting parameters, obtained by fitting the values of the tilt angle (see values reported in Figure 5b). The optimal values of these parameters in our case are γ = 0.25 and θ_0 = 24.1°.

3.2. X-ray Diffraction Results

Figure 6 shows a representative sequence of WA XRD patterns taken in the aligned nematic phase on cooling from the isotropic melt. While the onset of the nematic phase is observed at 105 °C, in good agreement with DSC and NMR data, no phase transition is observed until crystallization at 55 °C. The anisotropic patterns exhibit a pair of intense SA reflections centered on the meridional axis *m* (parallel to **n**) and a pair of weaker and broader WA reflections (only one shown in the figure, because of the pattern symmetry) centered on the equatorial axis *e* (orthogonal to **n**) at a scattering vector $q_0 \approx 1.43$ Å^{-1}. This value corresponds to a transverse intermolecular distance $d_t = 2\pi/q_0 \approx 4.4$ Å, a typical value for both calamitic and bent-core nematics. In particular, the WA reflections do not show the evident splitting observed in some laterally substituted BLCs, indicative of two different transverse intermolecular distances [2,47–49].

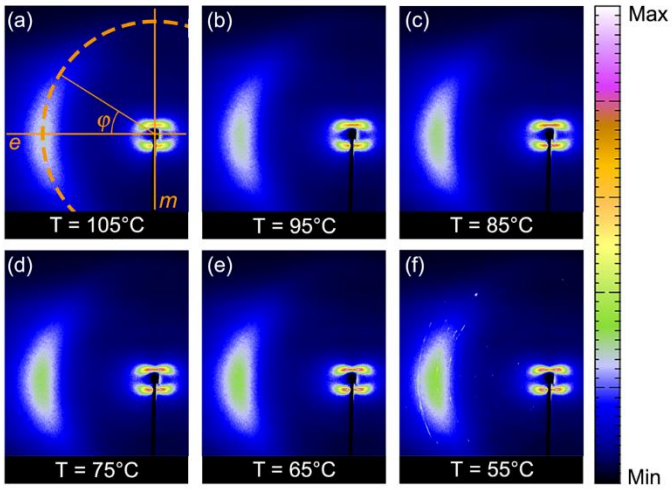

Figure 6. (**a**–**f**) WA XRD patterns taken in the nematic phase, aligned by a vertical magnetic field, at selected temperatures on cooling from the isotropic melt. Because of the pattern symmetry, only the left WA crescent is shown. In panel (**a**), lines *m* and *e* represent the meridional and equatorial axes, respectively, while the dashed arc indicates the measurement direction for the intensity profiles of the WA crescents as a function of the azimuthal angle φ. All patterns were background-corrected by subtracting the scattering from an empty capillary.

The position of the WA reflections, always lying on the equatorial axis, indicates the alignment of the molecular director **n** along the applied magnetic field **B** over the whole nematic temperature range. Analyzing the azimuthal broadening of the WA crescents is a well known means to evaluate the molecular orientational distribution function $f(\theta)$, θ which is here the angle between the long molecular axis and the molecular director **n**, and hence the orientational order parameter $<P_2>$, defined as

$$< P_2 >= \int_0^1 P_2(\cos\theta) f(\cos\theta) d(\cos\theta) \quad (4)$$

where P_2 is the second-order Legendre polynomial [50].

In the literature, different methods have been suggested to obtain $f(\theta)$ from the azimuthal intensity profile $I(\varphi)$ of the WA equatorial reflection, φ being the azimuthal angle on the detector measured with respect to the equatorial axis as shown in Figure 6a [51]. We followed the Kratky method described in [52], consisting in fitting the intensity profile $I(\varphi)$ with a truncated series of powers of cos φ. The series coefficients determined by the fitting procedure can be used to construct a series expansion of the orientational distribution function and hence, to evaluate $<P_2>$. Crucial to the method is a proper subtraction of the baseline intensity, usually evaluated at the edge of the integration region of the diffraction pattern. Applying this approach to the azimuthal intensity profiles taken along the dashed line shown in Figure 6a allowed us to obtain the values of $<P_2>$ shown in Figure 7.

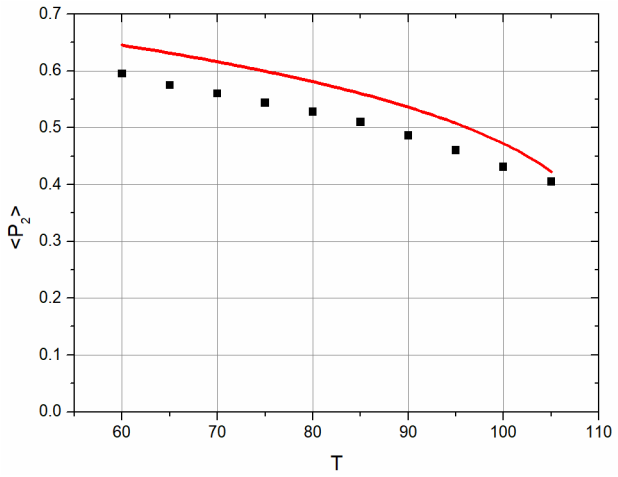

Figure 7. Orientational order parameter $<P_2>$ as a function of temperature T: data obtained by fitting the azimuthal intensity profile of the WA XRD reflection (black squares) and Maier-Saupe theoretical prediction (red line). For the latter, we used the approximate expression $< P_2 > = (1 - 0.98T/T_{NI})^{0.22}$, with T_{NI} indicating the clearing point.

Compared to the WA crescents, the SA reflections are significantly more intense (Figure 6), suggesting a high level of longitudinal molecular order. Figure 8a–g shows a sequence of XRD patterns taken with a larger sample-to-detector distance to expand the SA diffraction region. At high temperature, just below the clearing point, the SA pattern consists of two diffuse reflections centered on the meridional axis (Figure 8a). Upon cooling, they split to form a characteristic four-spot pattern (Figure 8b–g), a well known signature of skewed cybotactic order [15–17]—the presence in the nematic phase of nano-sized clusters of molecules featuring smectic C-like positional order. This behaviour is evidenced in Figure 9, reporting the intensity profiles of the SA reflections measured along the direction orthogonal to **B** and **n** (dashed line in Figure 8g): two peaks are evident for $T \leq 95$ °C, while at $T = 105$ °C, just below the clearing point, they merge almost completely into one broad peak and are not easily resolved.

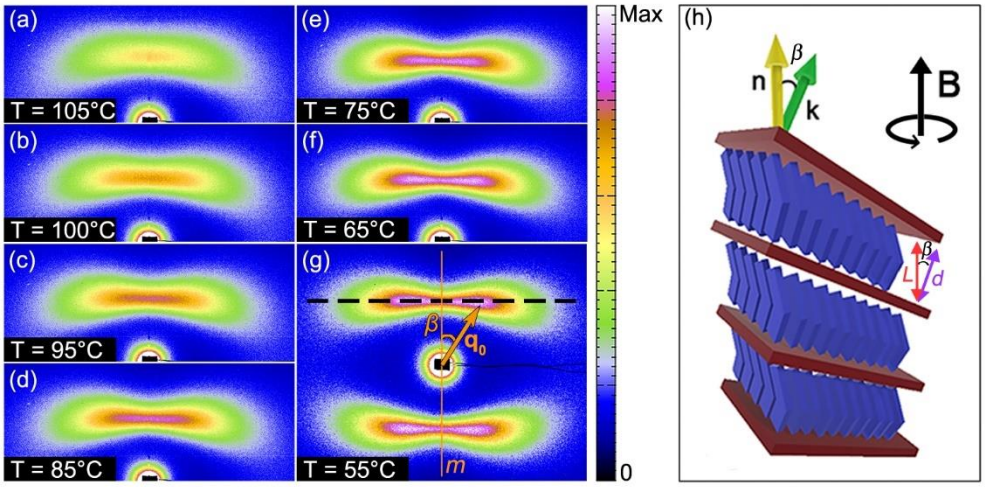

Figure 8. (**a**–**g**) SA XRD patterns taken in the nematic phase, aligned by a vertical magnetic field, at selected temperatures on cooling from the isotropic melt. Because of the pattern symmetry, only the upper half is shown in panels (**a**–**f**). Panel (**g**) also shows the scattering vector $\mathbf{q_0}$ associated to a diffraction peak, the angle β it forms with the meridional axis m (vertical orange line), and the measurement direction for the transverse intensity profiles of the SA peaks (black dashed line). (**h**) Schematic representation of a cybotactic cluster: β is the angle between the molecular director **n** and the normal to the smectic layers **k**, L is the molecular length and d the layer spacing. The clusters are isotropically distributed around the aligning magnetic field **B**.

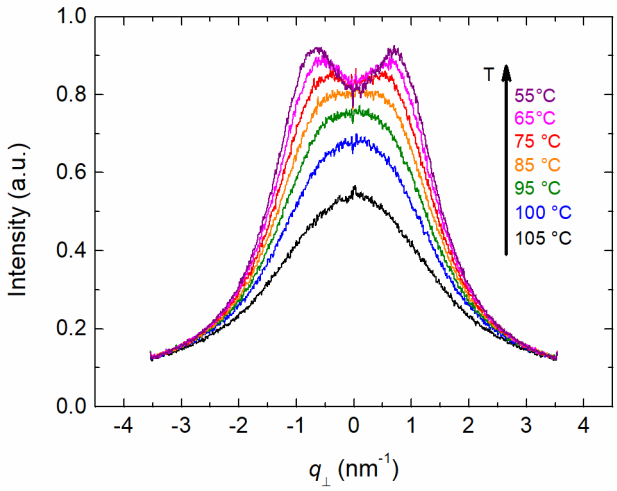

Figure 9. Transverse intensity profiles of the SA patterns shown in Figure 8, measured at different temperatures T along the black dashed line shown in Figure 8g.

According to the cybotactic model, the four-spot pattern (Figure 8g) reflects the smectic C-like structure of cybotactic clusters (Figure 8h) as follows [12,16,17]: the molecular director **n** is oriented by the magnetic field **B** along the meridional axis m, whereas the cluster transverse axes are isotropically oriented around **B**, as the scattering vector $\mathbf{q_0}$ associated to each SA reflection is perpendicular to the cluster smectic planes, the angle β between $\mathbf{q_0}$ and the meridional axis corresponds to the molecular tilt angle, i.e., the angle formed by the normal to the smectic planes **k** with **n**; the magnitude of $\mathbf{q_0}$ is determined by the layer spacing $d = 2\pi/q_0$; the molecular length L can be estimated as $d/\cos\beta$. The values of d, L and β obtained from the analysis of the SA four-spot patterns are shown in Figure 10. On cooling, the tilt angle increases from 23° at T = 100 °C to 34° at T = 55 °C; conversely, the layer spacing d decreases from 44 Å at T = 100 °C to 41 Å at T = 55 °C, while the molecular length L remains approximately constant over the nematic range with a value of ~49 Å, in good agreement with

the expected value for a fully extended molecular conformation. At T = 105 °C, β cannot be safely evaluated because of the almost compete overlap of the small-angle peaks: short-range positional order evolves towards normal, i.e., smectic A-like, cybotaxis on approaching the clearing point. Overall, the dependence on the temperature of these structural parameters is similar to that reported for other bent-core nematics [12,16,17].

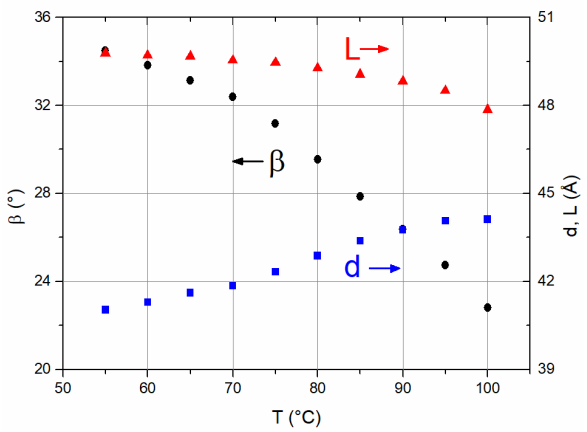

Figure 10. Molecular tilt angle β (black circles), layer spacing d (blue squares) and molecular length L (red triangles) as a function of the temperature T. Data obtained from the analysis of the SA diffraction patterns as described in the text.

Finally, the spatial extent of cybotactic order along the directions parallel and orthogonal to **n** can be estimated by means of the correlation lengths $\xi_{\parallel,\perp} = 2/\Delta q_{\parallel,\perp}$, with $\Delta q_{\parallel,\perp}$ representing the four-spot full width at half maximum measured along the longitudinal ($\parallel$ **n**) and transverse ($\perp$ **n**) direction, respectively. As usual, for the cybotactic nematic phase of BLCs [12,16,17], the calculated correlation lengths are very short, of the order of one molecular length in the longitudinal direction and of a few intermolecular distances in the transverse direction, reflecting a very short-ranged positional order (Figure 11). In addition, the correlation lengths are weakly dependent on the temperature, with no evidence of critical behaviour at phase transitions, setting a fundamental difference between the cybotactic order of BLCs and that observed in conventional (calamitic) nematics, the latter typically showing a pre-transitional character [15].

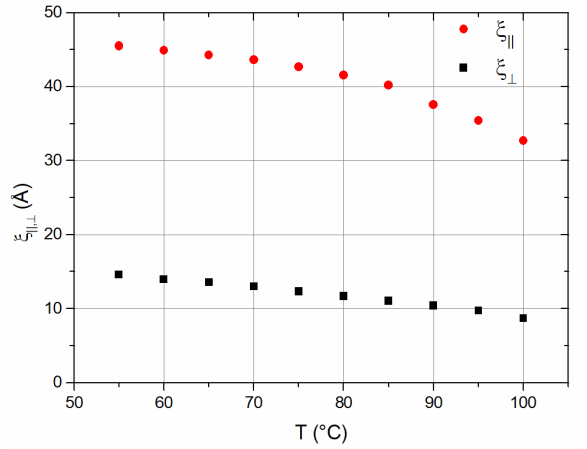

Figure 11. Longitudinal ($\xi_{\parallel}$, red circles) and transverse ($\xi_{\perp}$, black squares) positional correlation lengths as a function of the temperature T. Data obtained from the analysis of the SA diffraction patterns as described in the text.

3.3. Structure and Orientation: Final Discussion

The ^{2}H NMR results show that the two lateral deuterated rings give rise to the same NMR signals. Thus, they cannot be distinguished at the NMR time scale. This is in agreement with previous ^{13}C NMR results, where the two sets of ^{13}C signals relative to the two lateral wings, in particular, the aromatic carbons, are perfectly overlapped [37–39]. The ^{2}H NMR spectral shape, line-broadening and the values of the quadrupolar splittings as a function of temperature (Figures 3 and 4) give a clear indication of the occurrence of a transition around 70–71 °C between an aligned and nematic-like phase (at higher temperatures) and a more ordered, smectic-like or crystal-like phase (at lower temperatures).

The XRD data confirm the nematic nature of the high temperature phase, revealing a tilted (i.e., smectic C-like) cybotactic order. The structural properties of this cybotactic nematic phase are comparable to those observed in many other bent-core nematics, with positional correlation lengths that are very short and weakly dependent on the temperature and a molecular tilt angle (with respect to the layer normal) that increases as the temperature is lowered.

The orientational order parameter, $<P_2>$, estimated by XRD is quite close to the Maier-Saupe theoretical prediction (Figure 7), a remarkable result for a theory developed for rod-like mesogens. The values of $<P_2>$ are also in very good agreement with the order parameter of the central ring evaluated by ^{13}C NMR [38]. Unsurprisingly, the values are larger than the S_{zz} parameter estimated by ^{2}H NMR by about 0.15. This discrepancy reflects the different nature of the two order parameters, the former measuring the average orientation of the long molecular axis, the latter of the molecular wings, i.e., of the biphenyl *para*-axis, forming an angle α with the long molecular axis. A similar disagreement between NMR and XRD order parameters has been reported for other liquid crystal systems [53]. Following [38], α can be evaluated by comparing the two order parameters through the equation:

$$S_{zz} = < P_2 > \left(\frac{3\cos^2 \alpha - 1}{2} \right) \quad (5)$$

This expression leads to values of α ranging from 31° at 105 °C to 23° at 70 °C, corresponding to a bend-angle $\varepsilon = 180° - 2\alpha$ varying between 118° and 134°. As a comparison, previous works based on ^{13}C NMR provided a value of ε ranging from 122° to 128° for the not-labeled molecule [37–39], while DFT calculations indicate an even wider range of possible conformations, with α comprised between 110° and 140° [40].

The phase detected by NMR below 70 °C was not observed by the XRD methods, probably due to the metastability of the phase and the different experimental conditions of NMR and XRD experiments. Its nature could not be definitely assessed, but it likely represents a further crystalline phase, as also suggested by previous ^{13}C NMR investigations, which evidence the occurrence of several crystal-crystal phase transitions [37–39]. In this low temperature phase, ^{2}H NMR results indicate that the average direction of the deuterated biphenyl moieties is tilted with respect to the magnetic field **B** by about 24° at T~50 °C (Figure 5b). This behaviour could reflect a general propensity of the molecules for tilted arrangements, as in the skewed cybotactic nematic phase, as well as a conformational change of the BLC molecules. Previous works based on ^{13}C NMR [37–39] show that **10DClPBBC** is characterized by a large temperature dependence of the fragment biaxility of both the central and lateral aromatic rings and a variable molecular bending angle. These two structural features could explain our ^{2}H NMR findings.

4. Conclusions

The peculiar properties of nematic BLCs depend on their complex structural features. These are defined by a hierarchy of order parameters, describing the orientational and positional order at different length scales, namely those of specific molecular fragments, of the molecule principal axes, of nanosized molecular aggregates (cybotactic clusters), of the molecular director(s). Here, we have shown how ^{2}H NMR and XRD techniques can be conveniently combined to provide information on all these levels of

intra- and inter-molecular order, ultimately leading to a deeper insight into the fundamental features of BLCs' unconventional nematic phase.

Author Contributions: Conceptualization, F.V., O.F. and V.D.; Data curation, M.G., F.C.A., F.V. and V.D.; Formal analysis, M.G.; Investigation, F.V. and O.F.; Methodology, M.G., F.V., O.F. and V.D.; Supervision, V.D.; Validation, V.D.; Writing—original draft, F.V. and V.D.; Writing—review and editing, M.G., F.C.A., F.V. and O.F. All authors have read and agreed to the published version of the manuscript.

Funding: This research received no external funding.

Acknowledgments: M.G. and V.D. thank Fodor-Csorba (from Research Institute for Solid State Physics and Optics of the *Hungarian* Academy of Sciences, Budapest, Hungary) for providing the original BLC sample. F.V., F.C.A. and O.F. thank the staff of beamline BM26B-DUBBLE at the ESRF for technical support during XRD experiments and the staff of beamline BM28-XMaS for providing the superconducting magnet. Authors thank E.T. Samulski for helpful discussions.

Conflicts of Interest: The authors declare no conflict of interest.

References

1. Niori, T.; Sekine, F.; Watanabe, J.; Furukawa, T.; Takezoe, H.J. Distinct ferroelectric smectic liquid crystals consisting of banana shaped achiral molecules. *J. Mater. Chem.* **1996**, *7*, 1231. [CrossRef]
2. Harkins, R.; Tauscher, T.; Nguyen, J. Biaxial ordering in the supercooled nematic phase of bent-core mesogens: Effects of molecular symmetry and outer wing lateral groups. *Liq. Cryst.* **2019**. [CrossRef]
3. Begum, N.; Kaur, S.; Mohiuddin, G.; Nandi, R.; Gupta, S.P.; Rao, N.V.S.; Pal, S.K. Structural understanding, photoswitchability, and supergelation of a new class of four ring-based bent-shaped liquid crystal. *J. Phys. Chem. B* **2019**, *123*, 4443–4451. [CrossRef] [PubMed]
4. Alaasar, M.; Prehm, M.; Belau, S.; Sebastian, N.; Kurachkina, M.; Eremin, A.; Chen, C.L.; Liu, F.; Tschierske, C. Polar order, mirror symmetry breaking, and photoswitching of chirality and polarity in functional bent-core mesogens. *Chem. A Eur. J.* **2019**, *25*, 6362–6377. [CrossRef]
5. Pelzl, G.; Diele, S.; Weissflog, W. Banana-shaped compounds–A new field of liquid crystals. *Adv. Mater.* **1999**, *11*, 707. [CrossRef]
6. Eremin, A.; Jakli, A. Polar bent-shape liquid crystals–From molecular bend to layer splay and chirality. *Soft Matter* **2013**, *9*, 615–637. [CrossRef]
7. Lin, S.C.; Ho, R.M.; Chang, C.Y.; Hsu, C.S. Hierarchical superstructures with control of helicity from the self-assembly of chiral bent-core molecules. *Chem. A Eur. J.* **2012**, *18*, 9091–9098. [CrossRef]
8. Vita, F.; Adamo, F.C.; Francescangeli, O. Polar order in bent-core nematics: An overview. *J. Mol. Liq.* **2018**, *267*, 564–573. [CrossRef]
9. Acharya, B.R.; Primak, A.; Kumar, S. Biaxial nematic phase in bent-core thermotropic mesogens. *Phys. Rev. Lett.* **2004**, *92*, 145506. [CrossRef]
10. Madsen, L.A.; Dingemans, T.J.; Nakata, M.; Samulski, E.T. Thermotropic biaxial nematic liquid crystals. *Phys. Rev. Lett.* **2004**, *92*, 145505. [CrossRef]
11. Vita, F. Search for nematic biaxiality in bent-core mesogens: An X-ray diffraction perspective. *Liq. Cryst.* **2016**, *43*, 2254–2276. [CrossRef]
12. Francescangeli, O.; Stanic, V.; Torgova, S.I.; Strigazzi, A.; Scaramuzza, N.; Ferrero, C.; Dolbnya, I.P.; Weiss, T.M.; Berardi, R.; Muccioli, L.; et al. Ferroelectric response and induced biaxiality in the nematic phase of a bent-core mesogen. *Adv. Funct. Mater.* **2009**, *19*, 2592–2600. [CrossRef]
13. Francescangeli, O.; Vita, F.; Fauth, F.; Samulski, E.T. Extraordinary magnetic field effect in bent-core liquid crystals. *Phys. Rev. Lett.* **2011**, *107*, 207801. [CrossRef] [PubMed]
14. Gleeson, H.F.; Kaur, S.; Görtz, V.; Belaissaoui, A.; Cowling, S.; Goodby, J.W. The nematic phases of bent-core liquid crystals. *ChemPhysChem* **2014**, *15*, 1251–1260. [CrossRef]
15. Francescangeli, O.; Vita, F.; Samulski, E.T. The cybotactic nematic phase of bent-core mesogens: State of the art and future developments. *Soft Matter* **2014**, *10*, 7685–7691. [CrossRef]
16. Francescangeli, O.; Vita, F.; Ferrero, C.; Dingemans, T.; Samulski, E.T. Cybotaxis dominates the nematic phase of bent-core mesogens: A small-angle diffuse X-ray diffraction study. *Soft Matter* **2011**, *7*, 895–901. [CrossRef]
17. Francescangeli, O.; Samulski, E.T. Insights into the cybotactic nematic phase of bent-core molecules. *Soft Matter* **2010**, *6*, 2413–2420. [CrossRef]

18. Kim, Y.-K.; Cukrov, G.; Vita, F.; Scharrer, E.; Samulski, E.T.; Francescangeli, O.; Lavrentovich, O.D. Search for microscopic and macroscopic biaxiality in the cybotactic nematic phase of new oxadiazole bent-core mesogens. *Phys. Rev. E* **2016**, *93*, 062701. [CrossRef]
19. De Vries, A. Evidence for the existence of more than one type of nematic phase. *Mol. Cryst. Liq. Cryst.* **1970**, *10*, 31–37. [CrossRef]
20. Stojadinovic, S.; Adorjan, A.; Sprunt, S.; Sawade, H.; Jakli, A. Dynamics of the nematic phase of a bent-core liquid crystal. *Phys. Rev. E Stat. Nonlinear Soft Matter Phys.* **2002**, *66*, 060701. [CrossRef]
21. Domenici, V.; Geppi, M.; Veracini, C.A.; Blinc, R.; Lebar, A.; Zalar, B. Unusual dynamic behavior in the isotropic phase of banana mesogens detected by H-2 NMR line width and T-2 measurements. *J. Phys. Chem. B* **2005**, *109*, 769–774. [CrossRef] [PubMed]
22. Domenici, V.; Veracini, C.A.; Zalar, B. How do banana-shaped molecules get oriented (if they do) in the magnetic field? *Soft Matter* **2005**, *1*, 408–411. [CrossRef]
23. Domenici, V.; Veracini, C.A.; Fodor-Csorba, K.; Prampolini, G.; Cacelli, I.; Lebar, A.; Zalar, B. Banana-shaped molecules peculiarly oriented in a magnetic field: H-2 NMR spectroscopy and quantum mechanical calculations. *ChemPhysChem* **2007**, *8*, 2321–2330. [CrossRef] [PubMed]
24. Domenici, V. Dynamics in the isotropic and nematic phases of bent-core liquid crystals: NMR perspectives. *Soft Matter* **2011**, *7*, 1589–1598. [CrossRef]
25. Domenici, V.; Fodor-Csorba, K.; Frezzato, D.; Moro, G.; Veracini, C.A. Deuterium NMR evidences of slow dynamics in the nematic phase of a banana-shaped liquid crystal. *Ferroelectrics* **2006**, *344*, 263–272. [CrossRef]
26. Domenici, V.; Apih, T.; Veracini, C.A. Molecular motions of banana-shaped liquid crystals studied by NMR spectroscopy. *Thin Solid Films* **2008**, *517*, 1402–1406. [CrossRef]
27. Cifelli, M.; Domenici, V. NMR investigation of the dynamics of banana shaped molecules in the isotropic phase: A comparison with calamitic mesogens behaviour. *Phys. Chem. Chem. Phys.* **2007**, *9*, 1202–1209. [CrossRef]
28. Domenici, V.; Madsen, L.A.; Choi, E.J.; Samulski, E.T.; Veracini, C.A. Investigating the core moiety of banana-shaped liquid crystals using H-2 NMR coupled with quantum simulations. *Chem. Phys. Lett.* **2005**, *402*, 318–323. [CrossRef]
29. Cinacchi, G.; Domenici, V. Orientational ordering of a banana-shaped solute molecule in a nematic calamitic solvent by H-2-NMR spectroscopy: An indication of glasslike behavior. *Phys. Rev. E* **2006**, *74*, 030701. [CrossRef]
30. Domenici, V. Order and dynamics of rod-like and banana-shaped liquid crystals by H-2 NMR. *Pure Appl. Chem.* **2007**, *79*, 21–37. [CrossRef]
31. Cifelli, M.; Domenici, V.; Veracini, C.A. Recent advancements in understanding thermotropic liquid crystal structure and dynamics by means of NMR spectroscopy. *Curr. Opin. Colloid Interface Sci.* **2013**, *18*, 190–200. [CrossRef]
32. Figueirinhas, J.L.; Dong, R.Y. NMR of bent-core nematogens: A mini-review. *Magn. Reson. Chem.* **2014**, *52*, 614–624. [CrossRef] [PubMed]
33. Dong, R.Y. Recent developments in biaxial liquid crystals: An NMR perspective. *Int. J. Mod. Phys. B* **2010**, *24*, 4641–4682. [CrossRef]
34. Domenici, V. A brief overview of ^{2}H NMR experiments used to study the phase biaxiality in nematic liquid crystals. *Mol. Cryst. Liq. Cryst.* **2012**, *558*, 37–45. [CrossRef]
35. Cruz, C.; Figueirinhas, J.L.; Filip, D.; Feio, G.; Ribeiro, A.C.; Frère, Y.; Meyer, T.; Mehl, G.H. Biaxial nematic order and phase behavior studies in an organosiloxane tetrapode using complementary deuterium NMR experiments. *Phys. Rev. E* **2008**, *78*, 051702. [CrossRef]
36. Fodor-Csorba, K.; Vajda, A.; Jákli, A.; Slugovc, C.; Trimmel, G.; Demus, D.; Gács-Baitz, E.; Holly, S.; Galli, G. Ester type banana-shaped liquid crystalline monomers: Synthesis and physical properties. *J. Mater. Chem.* **2004**, *14*, 2499–2506. [CrossRef]
37. Xu, J.; Fodor-Csorba, K.; Dong, R.Y. Orientational ordering of a bent-core mesogen by two-dimensional ^{13}C NMR spectroscopy. *J. Phys. Chem. A* **2005**, *109*, 1998–2005. [CrossRef]
38. Dong, R.Y. A comparative ^{13}C NMR study of local ordering in a homologous series of bent-core liquid crystals. *J. Phys. Chem. B* **2009**, *113*, 1933–1939. [CrossRef]
39. Dong, R.Y.; Zhang, J.; Fodor-Csorba, K. On the carbon-13 chemical shift tensors of bent-core mesogens. *Chem. Phys. Lett.* **2006**, *417*, 475–479. [CrossRef]

40. Prampolini, G.; (C.N.R., Pisa, Italy). Personal communication, 2006.
41. Ghilardi, M. Studio Chimico Fisico di Un Cristallo Liquido Banana-Shaped in Fase Nematica Cibotattica. Ph.D. Thesis, University of Pisa, Pisa, Italy, 2015.
42. Thompson, P.B.J.; Bouchenoire, L.; Brown, S.D. New developments at the XMaS beamline for magnetic and high resolution diffraction. *AIP Conf. Proc.* **2004**, *705*, 428–431. [CrossRef]
43. Dong, R.Y. *Nuclear Magnetic Resonance of Liquid Crystals*; Springer: New York, NY, USA, 1997; ISBN 978-1-4612-1954-5.
44. Dong, R.Y. Advances in NMR studies of liquid crystals. *Annu. Rep. NMR Spectrosc.* **2004**, *53*, 68.
45. Xu, J.D.; Dong, R.Y.; Domenici, V.; Fodor-Csorba, K.; Veracini, C.A. C-13 and H-2 NMR study of structure and dynamics in banana B-2 phase of a bent-core mesogen. *J. Phys. Chem. B* **2006**, *110*, 9434–9441. [CrossRef] [PubMed]
46. Veracini, C.A. NMR spectra in liquid crystals. In *NATO ASI Series, Series C, 141*; Emsley, J.W., Ed.; Reidel: Dordrecht, The Netherlands, 1985; Chapter 5.
47. Vita, F.; Tauscher, T.; Speetjens, F.; Samulski, E.T.; Scharrer, E.; Francescangeli, O. Evidence of biaxial order in the cybotactic nematic phase of bent-core mesogens. *Chem. Mater.* **2014**, *26*, 4671–4674. [CrossRef]
48. Nguyen, J.; Wonderly, W.; Tauscher, T.; Harkins, R.; Vita, F.; Portale, G.; Francescangeli, O.; Samulski, E.T.; Scharrer, E. The effects of lateral halogen substituents on the low-temperature cybotactic nematic phase in oxadiazole based bent-core liquid crystals. *Liq. Cryst.* **2015**, *42*, 1754–1764. [CrossRef]
49. Glebowska, A.; Vita, F.; Francescangeli, O.; Dingemans, T.; Samulski, E. Molecular engineering room-temperature bent-core nematics. *Liq. Cryst.* **2015**, *42*, 829–839. [CrossRef]
50. Vita, F.; Hegde, M.; Portale, G.; Bras, W.; Ferrero, C.; Samulski, E.T.; Francescangeli, O.; Dingemans, T. Molecular ordering in the high-temperature nematic phase of an all-aromatic liquid crystal. *Soft Matter* **2016**, *12*, 2309. [CrossRef]
51. Agra-Kooijman, D.M.; Fisch, M.R.; Kumar, S. The integrals determining orientational order in liquid crystals by x-ray diffraction revisited. *Liq. Cryst.* **2017**, *45*, 680–686. [CrossRef]
52. Sims, M.T.; Abbott, L.C.; Richardson, R.M.; Goodby, J.W.; Moore, J.N. Considerations in the determination of orientational order parameters from X-ray scattering experiments. *Liq. Cryst.* **2019**, *46*, 11–24. [CrossRef]
53. Vita, F.; Adamo, F.C.; Pisani, M.; Heist, L.M.; Li, M.; Hegde, M.; Dingemans, T.J.; Samulski, E.T.; Francescangeli, O. Liquid crystal thermosets. A new class of high-performance materials. *Liq. Cryst.* **2019**. [CrossRef]